Acute and Subacute Effects of Irreversible Electroporation on Nerves: Experimental Study in a Pig Model[1]

Helmut Schoellnast, MD[2]
Sebastien Monette, DMV, MVSc
Paula C. Ezell, DVM
Ajita Deodhar, MD
Majid Maybody, MD
Joseph P. Erinjeri, MD, PhD
Michael D. Stubblefield, MD
Gordon W. Single, Jr, BS
William C. Hamilton, Jr, MBA, BS
Stephen B. Solomon, MD

Purpose: To evaluate whether irreversible electroporation (IRE) has the potential to damage nerves in a porcine model and to compare histopathologic findings after IRE with histopathologic findings after radiofrequency ablation (RFA).

Materials and Methods: This study was approved by the institutional animal care and use committee. Computed tomography (CT)-guided IRE of 11 porcine sciatic nerves was performed in nine pigs, and histopathologic analysis was performed on the day of ablation or 3, 6, or 14 days after ablation. In addition, acute RFA of six porcine sciatic nerves was performed in six pigs that were harvested on the day of ablation. All nerves and associated muscles and tissues were assessed for histopathologic findings consistent with athermal or thermal injury, respectively, such as axonal swelling, axonal fragmentation and loss, Wallerian degeneration, inflammatory infiltrates, Schwann cell proliferation, and coagulative necrosis. The percentage of fascicles affected was recorded.

Results: All nerves had an axonal injury. The percentage of affected nerve fascicles after IRE was 50%–100%. Axonal swelling and perineural inflammatory infiltrates were detectable at every time point after ablation. Axonal fragmentation and loss, macrophage infiltration, and Schwann cell proliferation were found 6 and 14 days after ablation. Distal Wallerian axonal degeneration was observed 14 days after ablation. The endoneurium and perineurium architecture remained intact in all cases. RFA specimens at the day of ablation revealed acute coagulative necrosis associated with intense basophilic staining of extracellular matrix, including collagen of the perineurium and epineurium consistent with thermal injury.

Conclusion: IRE has the potential to damage nerves and may result in axonal swelling, fragmentation, and distal Wallerian degeneration. However, preservation of endoneurium architecture and proliferation of Schwann cells may suggest the potential for axonal regeneration. In contrast, RFA leads to thermal nerve damage, causing protein denaturation, and suggests a much lower potential for regeneration.

[1] From the Department of Radiology (H.S., A.D., M.M., J.P.E., S.B.S.), Laboratory of Comparative Pathology (S.M.), Research Animal Resource Center (P.C.E.), and Department of Neurology (M.D.S.), Memorial Sloan-Kettering Cancer Center, 1275 York Ave, New York, NY 10065; and AngioDynamics, Queensbury, NY (G.W.S., W.C.H.). Received December 21, 2010; revision requested February 4, 2011; revision received March 14; accepted April 2; final version accepted April 13. **Address correspondence to** S.B.S. (e-mail: *solomons@mskcc.org*).

[2] **Current address:** Department of Radiology, Medical University of Graz, Graz, Austria.

Irreversible electroporation (IRE) refers to permanent permeabilization of the cell membrane by electric fields and is thought to be related to the formation of nanoscale defects or pores in the cell membrane, from which the term *poration* was derived (1,2). IRE has emerged as a promising technique for tumor ablation, with negligible thermal injury to tissues and without the extent of damage being influenced by heat sink of flowing blood, as is seen with thermal ablation (3). The finding that IRE can be used for ablation of substantial volumes of tissue has been confirmed in small studies (4) and large animal models in different organs (5–8). IRE does not result in destruction of connective tissue or denaturation of collagen typical of thermal ablation (7,8). This selective cell destruction may have important clinical implications, such as decreasing the incidence of bile duct, urethral, or renal collecting system damage in IRE ablation of the liver, prostate, or kidney, respectively (7,8).

IRE ablation has been evaluated in clinical studies with a percutaneous approach (7,9). Onik et al (10) performed IRE of the prostate in dogs and confirmed that there is complete cell death within the ablation zone. In one of these dogs, the lesion was intentionally made to include the neurovascular bundle, and the authors reported that the nerve was unaffected by IRE. This finding is in contrast to cryoablation findings. Cryoablation is a commonly used tool in focal treatment of prostate cancer that variably damages these neural structures. By sparing the neurovascular bundle during IRE of the prostate, one could potentially preserve potency and urinary function and thereby maintain quality of life in these patients. Furthermore, preservation of neural function would enable IRE ablation to be used as a treatment tool in any adjacent tumor to overcome the nerve damage seen with radiofrequency ablation (RFA) and cryoablation. However, the effect of IRE on the neurovascular bundle was assessed previously in a canine model (10). Thus, the aim of our study was to determine whether IRE has the potential to damage nerves in a porcine model and to compare histopathologic findings in nerves after IRE with histopathologic findings in nerves after treatment with RFA.

Advances in Knowledge

- Irreversible electroporation (IRE) ablation has the potential to damage nerves.
- Histomorphology of nerves after ablation with IRE suggests a potential for nerve regeneration.

Materials and Methods

This study was supported by AngioDynamics, who provided the IRE equipment. Two authors (G.W.S., W.C.H.) are employees of AngioDynamics. Those authors who are not employees of AngioDynamics (H.S., S.M., P.C.E., A.D., M.M., J.P.E., M.D.S., and S.B.S.) had control over the inclusion of any data and information that might have presented a conflict of interest for the authors who are employees of AngioDynamics.

Animals

The study was approved by the institutional animal care and use committee. Percutaneous computed tomography (CT)-guided IRE of 11 sciatic nerves (seven right nerves, four left nerves) and CT-guided RFA of six sciatic nerves (three right nerves, three left nerves) were performed in 15 Yorkshire pigs (weight range, 35–45 kg) from two suppliers (Archer Farms, Darlington, Md; Animal Biotech Industries, Danboro, Pa). IRE of one sciatic nerve was performed in seven pigs, IRE of both sciatic nerves was performed in two pigs, and RFA of one sciatic nerve was performed in six pigs. Each procedure started with premedication with tiletamine hydrochloride and zolazepam hydrochloride (Telazol; Fort Dodge Animal Health, Fort Dodge, Iowa) (4.4 mg per kilogram of body weight) administered intramuscularly and after intubation. General anesthesia was maintained with continuous inhalation of 1.5%–3% isoflurane. Buprenorphine (0.01 mg/kg) was given via intramuscular injection before the start of each procedure. Postprocedural pain was managed with intramuscular buprenorphine (0.01 mg/kg) and oral meloxicam (0.4 mg/kg). In the postprocedural course, the ablation site was assessed for bruising and warmth. The day on which the animal was able to stand without assistance and the day on which the animal was able to bear weight on the treated limb were recorded. Euthanasia time points were determined by clinical signs and with the aim to collect samples of lesions at different stages. Euthanasia was performed with an intravenous injection of pentobarbital sodium (87 mg/kg) and phenytoin sodium (11 mg/kg) (Euthasol; Vibrac AH, Fort Worth, Tex).

The sciatic nerves were harvested for histopathologic evaluation on the day of IRE ablation (six nerves in six pigs) or 3 (one nerve in one pig), 6 (two nerves in two pigs), or 14 (two nerves in two pigs) days after IRE ablation. After RFA, all nerves were harvested on the same day for humane reasons because one can assume that severe damage of the nerve has occurred after thermal ablation. Two unablated sciatic nerves were used for comparison.

IRE Ablation

Pigs were anesthetized and placed on the CT table (LightSpeed 16; GE Healthcare, Milwaukee, Wis) in a lateral position. Noncontrast CT of the pelvis was performed to identify the sciatic nerve and to plan the level and position of

Published online before print
10.1148/radiol.11103505 **Content code:** NR

Radiology 2011; 260:421–427

Abbreviations:
IRE = irreversible electroporation
RFA = radiofrequency ablation

Author contributions:
Guarantors of integrity of entire study, H.S., M.D.S., S.B.S.; study concepts/study design or data acquisition or data analysis/interpretation, all authors; manuscript drafting or manuscript revision for important intellectual content, all authors; manuscript final version approval, all authors; literature research, H.S., S.M., M.M.; experimental studies, H.S., S.M., P.C.E., M.M., M.D.S., G.W.S., W.C.H., S.B.S.; and manuscript editing, H.S., S.M., P.C.E., A.D., M.M., J.P.E., M.D.S., G.W.S.

Potential conflicts of interest are listed at the end of this article.

IRE electrode entry. The skin overlying the entry position of the electrodes was shaved and sterilized in the usual fashion with alcohol and betadine. Two single monopolar electrodes (Nano-Knife; AngioDynamics) were placed with CT guidance so that the sciatic nerve was bracketed between the active lengths of the electrodes (Fig 1). Ablation was performed by using active electrode exposure of 2 cm, electrode spacing of 0.9–1.5 cm, voltage of 1350–2250 V (voltage was chosen to keep a constant voltage per distance in tissue of 1500 V/cm), and pulse length of 70 μsec. Two ablations were performed per nerve with 90 pulses each with a change in the direction of the polarity to simulate the ablation protocol used in the prostate in which a neurovascular bundle may be ablated twice (a worst-case scenario). Pancuronium (0.15 mg/kg) was administered intravenously 10 minutes before ablation to reduce muscle contractions during application of the electrical pulses. The adequacy of muscle relaxation was checked with a test pulse before ablation. Correct needle placement was ensured before each ablation, and needle displacement due to muscle contraction was ruled out after each ablation with CT.

RFA Technique

Guidance for RFA (Boston Scientific, Natick, Mass) was performed in the same manner as was guidance for IRE ablation. Three ablations cycles were performed after CT-guided nerve block with administration of 0.25% bupivicaine via a 2-cm-diameter tip exposed only 1 cm. Ablation started at 20 W, and power was increased by 10 W every 30 seconds until a sudden and major rise in impedance.

Histopathologic Analysis

Histopathologic analysis was performed by a veterinary pathologist (S.M.) with 10 years of experience.

Immediately after euthanasia, a postmortem examination limited to the region of the ablation was performed. The portion of the middle gluteal muscle containing the ablation lesion and the adjacent sciatic nerve and associated adipose tissue and blood vessels were fixed by immersion in 10% neutral buffered formalin. A nerve specimen approximately 10 cm distal to the ablated area was also fixed in formalin. In two animals in which only one sciatic nerve was ablated, the contralateral nerve was harvested, fixed in formalin, and used as a control. Muscle, nerve, and associated tissues were routinely processed, embedded in paraffin, cut into 4-μm-thick slices, and stained with hematoxylin-eosin. Sections from selected specimens were also stained with Masson trichome for collagen and with Van Kossa for calcium. S100 immunostaining for Schwann cells was performed on selected sections by using polyclonal rabbit anti-S100a (Z0628; Dako, Carpinteria, Calif) and following the manufacturer's recommended protocol.

All nerves and associated muscles and tissues were assessed for histopathologic findings consistent with athermal or thermal injury, respectively, such as axonal swelling, axonal fragmentation and loss, inflammatory infiltrates, Schwann cell proliferation, and coagulative necrosis. The percentage of fascicles affected on transverse slices was recorded.

Results

Clinical Course

All animals that recovered had minimal bruising and warmth at the ablation site that resolved by 3 days after ablation. Each animal's recovery progressed differently in regards to the animal's ability to stand without assistance and bear weight on the treated limb. Of the five animals that recovered after the procedure, two were able to stand without assistance 1 day after the procedure, one was able to stand without assistance 2 days after the procedure, and one was able to stand without assistance 3 days after the procedure. One animal was still not able to stand without assistance 3 days after the procedure and was euthanized. Of the four animals that were able to stand without assistance after the procedure, one was able to bear weight on the treated limb on day 2 after the procedure; one, on day 3; one, on day 5; and one, on day 7.

Gross Pathology

IRE lesions.—At gross examination, a well-demarcated focal lesion was observed in the middle gluteal muscle, adjacent to the sciatic nerve. On the day of ablation and 3 days after ablation, the lesions were red, soft, and exuded serosanguineous fluid when sliced. Six and 14 days after ablation, the lesion was pale tan, firm, and contained numerous small (<1 mm in diameter) hard white foci of calcification. At all time points, the segments of the sciatic nerve adjacent to the muscle lesion (2–3 cm) appeared subjectively thickened (approximately 50% increase in thickness) compared with the control nerves.

RFA lesions.—Examination of ablated tissues revealed a well-demarcated lesion at the treatment site in the same location in the muscle. When sliced, the ablated muscle tissue was tan to brown, dull, and friable. This lesion included the nerve in all cases.

Histopathology

IRE lesions.—At histopathologic analysis, lesions were observed in all treated nerves at the site of ablation. All control nonablated nerves had normal histopathologic findings. Within the affected nerves, the percentage of fascicles affected by the lesion on the transverse slice varied from 50% to 100%. The unaffected fascicles were distributed geographically; if the injury was 50%, the affected half was on one side of the nerve and the unaffected half was on the other side. The histopathologic findings are summarized in Table 1. There was no obvious correlation between the clinical status of the animals after IRE and the percentage of fascicles affected (Table 2).

On the day of IRE ablation, all nerves showed perineural edema and infiltration by a few eosinophils and neutrophils. In five of six nerves, axonal swelling was observed. This finding was in contrast to findings in the control nerves, in which the axons were small and separated from the myelin sheath by a clear space, which was an expected artifact.

On day 3 after IRE ablation, myelin degeneration and perineural infiltration by a small number of neutrophils and eosinophils were observed. S100 immunostaining showed decreased protein expression around many axons when compared with that in the control nerve, indicating Schwann cell loss.

In addition to the changes described previously, on day 6 after IRE ablation, there was increased cellularity within the affected fascicles, characterized by cells with ovoid elongated nuclei and scant cytoplasm. One of two nerves showed fragmentation of axons and presence of phagocytes within ellipsoids. At this stage, loss of S100 staining around axons was observed and was more intense than that seen 3 days after IRE ablation. However, multifocal dense clusters of cells were seen. Some of these cell clusters demonstrated S100 expression, indicating proliferation of Schwann cells forming Buengner bands. Many other cell clusters were negative for S100, suggesting that fibroblast proliferation was also occurring.

The same changes were observed 14 days after ablation, with more extensive and advanced fragmentation of axons, infiltration by phagocytes, and endoneurial hypercellularity. A mild increase in perineurial collagen was observed. As on day 6, S100 immunostaining revealed that some cells present in high numbers within fascicles were positive and some were negative, suggesting proliferation of both Schwann cells and fibroblasts. However, the presence of multifocal thick bands of Schwann cell was more pronounced than that on day 6. Changes consistent with Wallerian degeneration were observed in the specimens obtained distal to the ablation site in both specimens on day 14.

Figure 2 shows the histopathogic findings in the nerves after IRE ablation over time. At all stages, the endoneurial architecture was preserved (Fig 3).

Histopathologic analysis of slices of the lesion in the adjacent skeletal muscle revealed a well-demarcated area of coagulative necrosis, edema, and hemorrhage in all cases. On day 3, the periphery of the lesion was infiltrated by macrophages. Calcification of necrotic

Figure 1

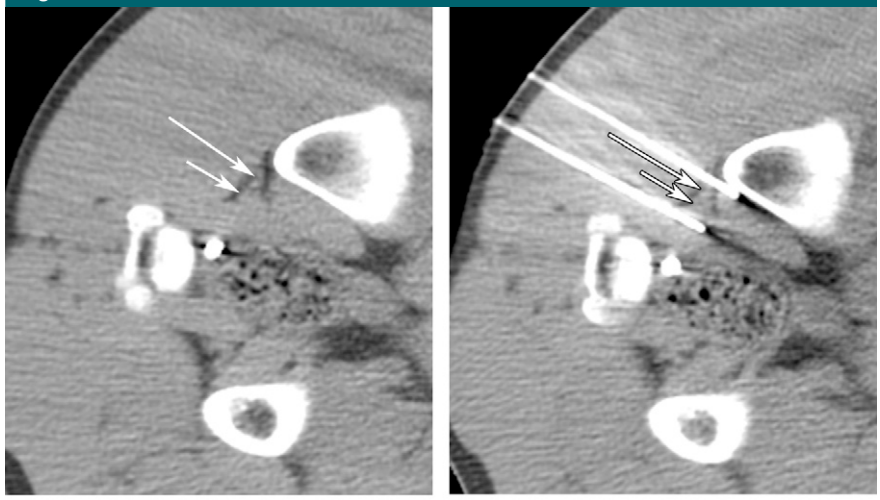

a. b.

Figure 1: **(a)** CT image before IRE ablation shows level of planned probe entry with right sciatic nerve (long arrow) and accompanying arteria comitans nervi ischiadici (short arrow) surrounded by fat tissue. **(b)** CT image after placement of IRE electrodes with right sciatic nerve (long arrow) and accompanying artery (short arrow) between electrode tips.

Table 1

Histopathologic Findings in Sciatic Nerves after IRE Ablation

Finding	Day 0	Day 3	Day 6	Day 14
Perineurial edema	6/6	0/1	0/2	0/2
Perineurial inflammatory infiltrate	6/6	1/1	2/2	2/2
Axonal swelling	5/6	1/1	2/2	2/2
Myelin ellipsoids	0/6	1/1	2/2	2/2
Axonal fragmentation and loss	0/6	0/1	1/2	2/2
Phagocytes	0/6	0/1	1/2	2/2
Schwann cell and fibroblast hyperplasia	0/6	0/1	2/2	2/2
Perineurial fibrosis	0/6	0/1	0/2	2/2
Distal Wallerian degeneration	0/6	0/1	0/2	2/2

Note.—The first number is the number of nerve specimens that showed a specific histopathologic finding. The second number is the number of total specimens examined.

Table 2

Correlation between Percentage of Fascicles Affected by IRE and Clinical Status after IRE

Animal No.	Fascicles Affected (%)	No. of Days Until Standing after IRE	No. of Days Until Bearing Weight after IRE
1*	50	NA	NA
2	50	2	5
3	90	3	7
4	90	1	3
5	50	1	2

Note.—Animals listed in this table are animals that recovered after IRE and were kept alive for up to 14 days. NA = not applicable.

* This animal was unable to stand without assistance up to 3 days after the procedure and was euthanized.

Figure 2

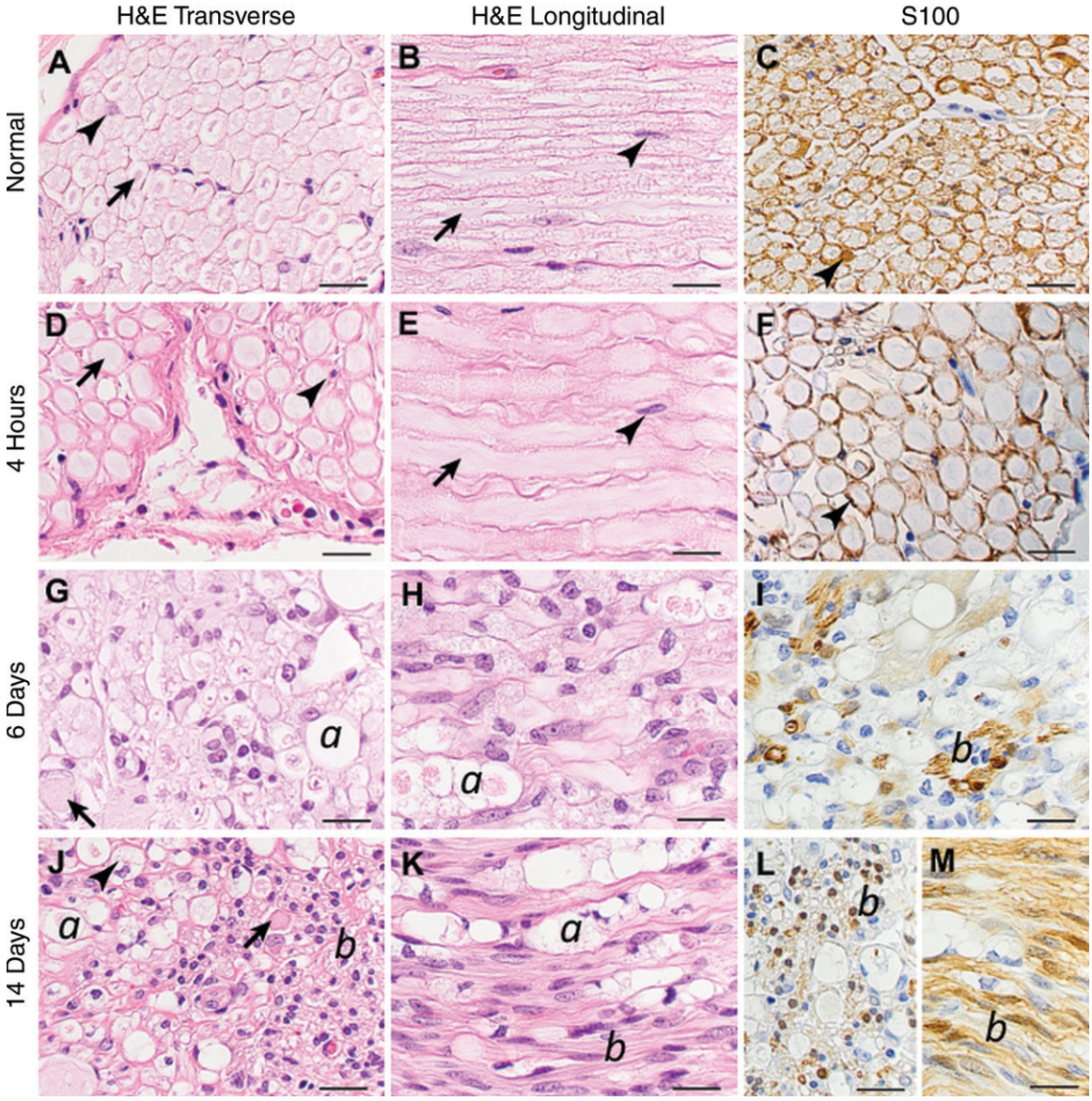

Figure 2: Histopathologic slides after IRE ablation. *H&E* = hematoxylin-eosin stain, *S100* = S100 immunohistochemical stain. S100-stained sections are transverse, except *M*, which is longitudinal. Original magnification, ×600; scale bar = 20 μm. *A–C*, Slides of untreated nerve show normal morphology. Arrows = axons, arrowheads = Schwann cells surrounding myelinated axons and characterized by cytoplasmic and nuclear S100 staining. *D–F*, Axonal swelling is seen (arrows). Schwann cell morphology and number are normal (arrowheads). *G–I*, Swollen axons (arrow) and ellipsoids containing axonal and myelin debris *(a)* are seen. Increased cellularity is also seen. Most nuclei are S100 negative, but small clusters of S100-positive Schwann cells are observed on occasion *(b)*. *J–L*, Swollen axons (arrow) and ellipsoids *(a)* that occasionally contain phagocytes with foamy cytoplasm (arrowhead). Prominent thick bands of S100-positive Schwann cells *(b)* are present.

fibers, characterized by basophilic stippling at hematoxylin-eosin staining and black stippling at Van Kossa staining, was observed on days 3 and 6. On days 6 and 14, there was infiltration by a higher number of macrophages and numerous fibroblasts and evidence of fibroplasia progressing from the periphery to the center of the lesion and gradually replacing the necrotic tissue.

The arteria comitans nervi ischiadici, a branch of the inferior gluteal artery that accompanies the sciatic nerve, was normal from the day of ablation to 6 days after ablation and showed hyperplasia of the intima and media 14 days after ablation.

RFA lesions.—Muscle and nerve specimens obtained on the day of RFA revealed a well-demarcated area of acute coagulative necrosis characterized by

Figure 3

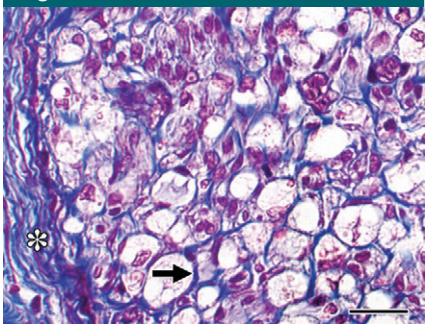

Figure 3: Histopathologic slide obtained 14 days after IRE ablation. Endoneurial (arrow) and epineurial (*) extracellular matrix has a normal architecture. Collagen is blue. (Masson trichrome stain; original magnification, ×600.) Scale bar = 20 μm.

Figure 4

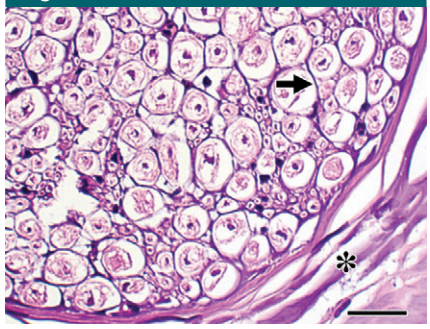

Figure 4: Histopathologic slide obtained 4 hours after RFA. Endoneurial (arrow) and perineurial (*) collagen shows intense basophilic staining, compatible with thermal injury, which indicates protein denaturation. Compare this image with images of the eosinophilic normal nerve (Fig 2, *A*) and the eosinophilic nerve 4 hours after IRE ablation (Fig 2, *D*). Nuclei are pyknotic. (Hematoxylin-eosin stain; original magnification, ×600.) Scale bar = 20 μm.

nuclear pyknosis and cytoplasmic hypereosinophilia associated with intense basophilic staining of the extracellular matrix, including collagen of the perineurium and epineurium. These findings were compatible with a thermal injury (Fig 4).

Discussion

In our study, all nerves showed histopathologic signs of damage after IRE, albeit with variability in the percentage of fascicles affected. This does not support the initial findings of Onik et al (10), who reported that IRE had no effect on nerves.

In our study, axonal swelling was observed in all treated specimens at all time points, and axonal fragmentation and loss were observed 6 and 14 days after ablation, leading to Wallerian degeneration of the nerve distal to the ablation site 14 days after ablation. However, most interestingly, the external architecture of the nerve remained intact in all cases, and Schwann cell hyperplasia was observed 6 and 14 days after ablation, suggesting that there is potential for axonal regeneration. Schwann cells play an important role in nerve regeneration at the site of injury (11–13).

After nerve transection, axons of the proximal segment begin to sprout and advance through the transection site only to be pruned down when the endoneurial tubes of the distal stump are reached (14–16). The distal segment undergoes a slow process of degeneration known as Wallerian degeneration. This process starts immediately after injury and involves myelin breakdown. Schwann cells and macrophages are recruited to the injury site, where they phagocytize myelin and cellular debris. Disintegration of axons and the loss of axon–Schwann cell contact is a signal that initiates the proliferation of Schwann cells, which organize themselves into columns (Buengner bands), and the regenerating axons associate with them by growing distally between their basal membranes (17). Thus, although IRE led to axonal fragmentation in our study, there may be potential for axonal regeneration; this supposition is based on the preserved architecture of the endoneurium and the proliferation of Schwann cells.

In contrast to IRE ablation, hematoxylin-eosin staining of the sciatic nerve after RFA showed intense basophilic staining of the collagen of the perineurium and epineurium consistent with thermal injury, which is protein denaturation. If the collagen has undergone denaturation, it probably cannot serve its function anymore; therefore, the radiofrequency ablated nerve would probably have much less potential for regeneration. This is also supported by the findings of Bunch et al (18), who performed RFA of the phrenic nerve in dogs and reported that in all nerves with permanent injury, the histopathologic findings were consistent with acute thermal injury.

After IRE ablation, the muscles showed necrosis, hemorrhage, and edema at all time points and infiltration with macrophages and fibroblasts beginning 3 days after ablation. Fibrosis was seen at later time points. Fibrinoid necrosis of small vessels was seen in some cases and was also previously reported (4,10). The ablated zone was well demarcated with an abrupt transition between the ablated and unablated areas concordant with previous reports (2,9,10). The accompanying artery to the sciatic nerve was normal at day 3 and day 7 and showed intimal and media hyperplasia and regeneration 14 days after ablation. This is in accordance with the findings of Lee et al (9), who performed IRE of the liver in pigs and reported that some intrahepatic arteries in the ablation field showed signs of vasculitis.

The main parameter affecting the results of IRE ablation is electric field strength, whereas trains of a large number of short pulses result in the best antitumor effects (19,20). The IRE parameters used in our study are widely in accordance with the parameters used in in vitro and in vivo studies in which complete ablation has been reported by using a field magnitude of 1000–2500 V/cm (7,9,10,20). One possible explanation for the discrepancy between our findings and the findings of Onik et al (10) is the electric fields applied to the nerve. Although Onik et al (10) applied 2000 V/cm in their experiment and we applied 1500 V/cm in our study, the effective voltage applied to the nerve by Onik et al may have actually been lower than that used in our study. It is important to note that the actual electric field that develops in the area between the two electrodes varies strongly with the position of the electrodes. In fact, the regions with the largest electric fields occur immediately adjacent to the needle electrodes. Edd and Davalos (21) applied a voltage-to-distance ratio of 1000 V/cm and calculated that the actual electric field adjacent to the electrodes

was 1600 V/cm. In our study, both electrodes were placed with CT guidance, and the anatomic course of the sciatic nerve close to the acetabulum may have led to some cases in which the nerve was closer to one electrode than the other. One can assume a high electric field in this location. The fact that 50%–100% of fascicles were affected and that the distribution between affected and unaffected fascicles was geographic may reflect the distance of the fascicles to the electrodes. In addition, the induced potential depends on the ohmic characteristics of the tissue and can differ in heterogeneous tissues (22). This may also have led to some variation in electric field strength between our study and the study by Onik et al (10), since IRE ablation was performed in different body regions and nerves, respectively.

Although damage was observed in each sciatic nerve examined, most pigs recovered quickly after the procedure and were able to stand without assistance and bear weight on the treated limb a few days after the procedure. This may be explained by the fact that the gluteal muscles and the extensors and adductors of the thigh are not affected by palsy of the sciatic nerve.

This study had several limitations. The small sample size and site-specific nature of the ablation make it difficult to extrapolate these results to nerve injury during IRE of other parts of the body. Although RFA leads to thermal nerve damage and is an established treatment tool for pain management (18,23), the lack of control lesions that underwent RFA at different time points is a further limitation of this study. In consideration of the known clinical effects of RFA on nerves, all animals were euthanized after ablation for humane reasons.

Practical application: Our results show that IRE has the potential to damage nerves while leaving the external architecture of the nerve intact. Further studies are necessary to evaluate the influence of IRE parameters on the incidence of nerve damage and to evaluate how the preservation of neural architecture with IRE potentiates nerve regeneration.

Disclosures of Potential Conflicts of Interest: H.S. No potential conflicts of interest to disclose. **S.M.** No potential conflicts of interest to disclose. **P.C.E.** No potential conflicts of interest to disclose. **A.D.** Financial activities related to the present article: institution received a research grant for irreversible electroporation. Financial activities not related to the present article: none to disclose. Other relationships: none to disclose. **M.M.** No potential conflicts of interest to disclose. **J.P.E.** No potential conflicts of interest to disclose. **M.D.S.** No potential conflicts of interest to disclose. **G.W.S.** Financial activities related to the present article: none to disclose. Financial activities not related to the present article: is employed by AngioDynamics. Other relationships: none to disclose. **W.C.H.** Financial activities related to the present article: none to disclose. Financial activities not related to the present article: is employed by and holds stock/stock options with AngioDynamics. Other relationships: none to disclose. **S.B.S.** Financial activities related to the present article: institution received an unrestricted grant and equipment from AngioDynamics. Financial activities not related to the present article: is a consultant for GE Healthcare and Johnson & Johnson, institution received a grant from GE Healthcare. Other relationships: none to disclose.

References

1. Neumann E, Rosenheck K. Permeability changes induced by electric impulses in vesicular membranes. J Membr Biol 1972;10(3):279–290.
2. Rubinsky B. Irreversible electroporation in medicine. Technol Cancer Res Treat 2007;6(4):255–260.
3. Davalos RV, Mir ILM, Rubinsky B. Tissue ablation with irreversible electroporation. Ann Biomed Eng 2005;33(2):223–231.
4. Edd JF, Horowitz L, Davalos RV, Mir LM, Rubinsky B. In vivo results of a new focal tissue ablation technique: irreversible electroporation. IEEE Trans Biomed Eng 2006;53(7):1409–1415.
5. Deodhar A, Monette S, Single GW Jr, et al. Renal tissue ablation with irreversible electroporation: preliminary results in a porcine model. Urology 2010;77(3):754–760.
6. Lavee J, Onik G, Mikus P, Rubinsky B. A novel nonthermal energy source for surgical epicardial atrial ablation: irreversible electroporation. Heart Surg Forum 2007;10(2):E162–E167.
7. Lee EW, Chen C, Prieto VE, Dry SM, Loh CT, Kee ST. Advanced hepatic ablation technique for creating complete cell death: irreversible electroporation. Radiology 2010;255(2):426–433.
8. Rubinsky B, Onik G, Mikus P. Irreversible electroporation: a new ablation modality—clinical implications. Technol Cancer Res Treat 2007;6(1):37–48.
9. Lee EW, Loh CT, Kee ST. Imaging guided percutaneous irreversible electroporation: ultrasound and immunohistological correlation. Technol Cancer Res Treat 2007;6(4):287–294.
10. Onik G, Mikus P, Rubinsky B. Irreversible electroporation: implications for prostate ablation. Technol Cancer Res Treat 2007;6(4):295–300.
11. Son YJ, Thompson WJ. Schwann cell processes guide regeneration of peripheral axons. Neuron 1995;14(1):125–132.
12. Fu SY, Gordon T. Contributing factors to poor functional recovery after delayed nerve repair: prolonged denervation. J Neurosci 1995;15(5 Pt 2):3886–3895.
13. Fu SY, Gordon T. Contributing factors to poor functional recovery after delayed nerve repair: prolonged axotomy. J Neurosci 1995;15(5 Pt 2):3876–3885.
14. Donnerer J. Regeneration of primary sensory neurons. Pharmacology 2003;67(4):169–181.
15. Su HX, Cho EYP. Sprouting of axon-like processes from axotomized retinal ganglion cells induced by normal and preinjured intravitreal optic nerve grafts. Brain Res 2003;991(1-2):150–162.
16. Czaja K, Burns GA, Ritter RC. Capsaicin-induced neuronal death and proliferation of the primary sensory neurons located in the nodose ganglia of adult rats. Neuroscience 2008;154(2):621–630.
17. Geuna S, Raimondo S, Ronchi G, et al. Chapter 3: histology of the peripheral nerve and changes occurring during nerve regeneration. Int Rev Neurobiol 2009;87:27–46.
18. Bunch TJ, Bruce GK, Mahapatra S, et al. Mechanisms of phrenic nerve injury during radiofrequency ablation at the pulmonary vein orifice. J Cardiovasc Electrophysiol 2005;16(12):1318–1325.
19. Al-Sakere B, André F, Bernat C, et al. Tumor ablation with irreversible electroporation. PLoS ONE 2007;2(11):e1135.
20. Miller L, Leor J, Rubinsky B. Cancer cells ablation with irreversible electroporation. Technol Cancer Res Treat 2005;4(6):699–705.
21. Edd JF, Davalos RV. Mathematical modeling of irreversible electroporation for treatment planning. Technol Cancer Res Treat 2007;6(4):275–286.
22. Bertacchini C, Margotti PM, Bergamini E, Lodi A, Ronchetti M, Cadossi R. Design of an irreversible electroporation system for clinical use. Technol Cancer Res Treat 2007;6(4):313–320.
23. Golovac S. Radiofrequency neurolysis. Neuroimaging Clin N Am 2010;20(2):203–214.